Batteries & Supercaps

Research Article
doi.org/10.1002/batt.202400463

Chemistry Europe
European Chemical Societies Publishing

www.batteries-supercaps.org

Synergistic Dual Electrolyte System of LATP and In- Situ Solod-State PDOL System and its Improvement on the Performance of NCM811 Batteries

Jian-Hua Cao[+],[a] Peng Zhang[+],[a] Ya-kun Wang,[b] and Da-Yong Wu*[a]

1,3-Dioxolane (DOL) can undergo in-situ polymerization in batteries to form solid-state organic electrolyte PDOL. When applied to NCM811||Li battery system, PDOL electrolyte helps optimize the contact and interface stability between electrolyte and electrodes. This study explores the effects of PDOL with PE separators coated with $Li1_{.3}Al_{0.3}Ti_{1.7}(PO_4)_3$(LATP) on the performance of NCM811||Li batteries. 2,2,2-trifluoroethyl phosphite (DETFPi), was mixed with DOL at a 1:35 mass ratio. Then, $LiBF_4$ was used to initiate in-situ polymerization and thereby obtained DETFPi-PDOL electrolyte after 24 h at room temperature. The composite electrolyte exhibits enhanced ion conductivity (1.59×10^{-4} S cm^{-1}), high lithium ion transference number (0.78), wide electrochemical stability window (4.53 V), and high critical current density (2.2 mA cm^{-2}). Li||PDOL@LATP||Li battery shows extremely low overpotential (35 mV) after a constant current stable cycle of 500 h at 1.0 mA cm^{-2}. After 500 cycles at 1 C, the remaining capacity is 153.9 mAh g^{-1} with a capacity retention of 82.1 % in NCM811||PDOL@LATP||Li batteries. This indicates that the LATP coating on the surface of the PE separator plays an important role in optimizing the performance of DETFPI-PDOL electrolyte batteries. LATP and DETFPI-PDOL are effective in improving the cycling stability, rate performance, and interface state of NCM811 batteries.

Introduction

Solidification is an important technological approach to enhance the safety of batteries under high energy density conditions[1–3] and holds promise for advancing the commercial application of metallic lithium anodes.[4,5] The key to achieving battery solidification lies in solid electrolyte materials and in-situ solidification technologies. Solid electrolytes are the core materials of solid-state batteries, primarily including inorganic solid electrolytes (ISE),[6] polymer solid electrolytes (SPE),[7] and their composition, the organic-inorganic composite electrolytes (CPE) with high ion conductivity and processability.[8–10] Predictably, novel composite solid electrolytes will continue to be discovered and invented in the future.[11–13]

In situ solidification is a technology in which the liquid precursor of polymer electrolyte solidifies and transforms into a solid electrolyte after being injected into the battery. It is the most promising method to improve the interface performance between the separator (electrolyte) and electrode without liquid electrolyte.[14–17] This technology involves replacing liquid electrolyte with liquid small-molecule precursor and injecting it into batteries that have assembled electrodes, so as to let it infiltrate into gaps between electrode material particles, pores in the separator, and interfaces between electrodes. Then, under specific light or thermal initiation conditions, polymerization occurs to form polymer solid electrolytes, which ensures good contact with both cathodes and anodes to effectively reduce interface resistance. In the field of lithium batteries, there are three methods in in-situ polymerization: separator-assisted in-situ polymerization, in-situ polymerization on electrode surfaces, and polymerization after artificially forming protective layers on electrode surfaces. Thereinto, separator-assisted in-situ polymerization involves process of filling precursors into a pre-assembled battery comprising anode, cathode, and separator, followed by the polymerization of precursors inside the sealed battery. During the whole process, separator helps provide dimensional stability and mechanical strength to polymer electrolytes and improve electrode-electrolyte interface contact between the anode and cathode. More importantly, this method is suitable for liquid battery assembly processes and therefore, compatible with the existing battery production equipment.[18]

1,3-Dioxolane (DOL) is an ether solvent that polymerizes at room temperature upon the initiation by certain cationic initiators. Polydioxolane (PDOL) after ring opening polymerization contains —O—CH_2— segments which is similar to PEO, exhibiting excellent lithium ion (Li^+) transport capability. Solid-state or gel-state PDOL electrolytes have also shown outstanding cycling performance,[19–24] thus attracting considerable research attention in recent years. However, its relatively low ionic conductivity and narrow electrochemical window limit its application in high-voltage cathodes. Li et al.[25] used $SnCl_4$ to initiate DOL polymerization, forming a LiCl/LiSn alloy composite protective layer on the lithium metal anode, thereby achieving

[a] J.-H. Cao,[+] P. Zhang,[+] D.-Y. Wu
Technical Institute of Physics and Chemistry, Chinese Academy of Sciences, 29 Zhong-Guan-Cun East Rd. Hai-Dian District, 100190 Beijing, China
E-mail: dayongwu@mail.ipc.ac.cn

[b] Y.-k. Wang
School of Foreign studies, China University of Political Science and Law, 102249 Beijing, China

[+] These authors contributed equally to this work.

Supporting information for this article is available on the WWW under https://doi.org/10.1002/batt.202400463

Research Article
doi.org/10.1002/batt.202400463
Chemistry Europe
European Chemical Societies Publishing

high ionic conductivity (>2 mS cm^{-1}) and a wide electrochemical window (4.7 V). Huang et al.[26] introduced high-voltage stable plasticizers fluoroethylene carbonate (FEC) and succinonitrile (SCN) into PDOL electrolytes, achieving an ion conductivity of 1.95×10^{-4} S cm^{-1} and an electrochemical window of 4.43 V.

The development of solid-state batteries is progressing from separators to separators-free designs.[27] In-situ solidification technologies can be applied into various occasions, from polyolefin separators to separators coated with ion conductors, and further to ion conductor isolation-conduction layers, and play a promoting role.[28–32] Polymer electrolytes have already been used in batteries with polyolefin separators,[33–35] meanwhile the idea of using ion conductor-coated separators has recently sparked interest among researchers,[36,37] although with many practical challenges to be addressed.

Based on our previous researches on sacrificial additives to enhance performance of PDOL and lithium metal battery, we intend to explore the interaction between PDOL and inorganic ion conductor-coated separators, along with their effects on the performance of NCM811||Li and NCM811||C batteries.

Experimental Section

Material

Dichloromethane (AR, 99.9%), triethylamine (AR), and 4-(dimethylamino)pyridine (DMAP, AR) were purchased from Beijing Enokai Technology Co., Ltd. 2,2,2-Trifluoroethanol (TFEA, 99.5%) was purchased from Shanghai McLean Biochemical Technology Co., Ltd. Diethyl phosphorochloridate (95%) was purchased from Shanghai Titan Technology Co., Ltd. Lithium tetrafluoroborate ($LiBF_4$, 99.9%), 1,3-dioxolane (DOL, 99.8%), trimethylolpropane tri(methacrylate) (TTE), dimethyl carbonate (DMC, 99.9%), and ethylene carbonate (EC, 99.5%) were purchased from Shanghai Aladdin Biochemical Technology Co., Ltd. LATP particles were provided by the Institute of Physics, Chinese Academy of Sciences. BYK LPC22092, BYK-LPC22346, BYK-1785, BYK-LPX20990, Laponite RD were purchased from BYK Chemistry. NCM811, Super-P, polyvinylidene fluoride (PVDF, Arkema HSV900 from France), lithium foils (thickness 0.45 mm, diameter 15.6 mm), and button cell cases, along with other battery materials, were purchased from Shenzhen Kejing Zhida Co., Ltd. PE separators (thickness 9 μm, porosity 40%) were purchased from Hebei Jinli New Energy Technology Co., Ltd. Powder materials were vacuum-dried at 100 °C for 12 hours before use, while other materials were used as received.

Synthesis and Preparation

Synthesis of Sacrificial Additive DETFPi

The sacrificial additive DETFPi, which was used to enhance the compatibility between PDOL electrolyte and cathode, was synthesized following the method reported in the literature.[32]

LATP-Coated PE Composite Separator

LATP Slurry

39.45 g of deionized water and 7.50 g of LATP were weighed into a beaker, followed by a sequential dropwise addition of 0.30 g of BYK LPC22092, 0.05 g of BYK 1785, 0.35 g of BYK-LPX20990, and 0.10 g of Laponite RD. The mixture was pre-dispersed using magnetic stirring at 300 rpm until no layering or precipitation was observed, resulting in a milky white slurry. This pre-dispersed slurry was further added to a ball milling jar containing 100 mL of zirconia balls at a ratio of 1:0.34 (slurry to balls) and ball milled at 300 rpm for 12 hours.The zirconia balls with diameters of 5, 8, and 10 mm in a 1:3:6 mass ratio were used for ball milling. After ball milling, the slurry was filtered through a 200 mesh sieve, and 2.00 g of BYK-LPC22346 binder was added to the filtrate. The mixture was stirred at 300 rpm for 2 hours to obtain LATP aqueous slurry.

Coating

The LATP slurry described above was blade-coated onto PE separators using a vacuum heat automatic film applicator (AFA-V, Dongguan Dali Instrument Co., Ltd.). The coating parameters were set as follows: coating speed of 50 cm min^{-1} and coating thickness of 5 μm. The LATP slurry was first coated on one side of the PE separator, and after dried, coated on the other side. The coated PE separator was finally dried at 60 °C for 6 hours to obtain LATP/PE/LATP composite separator.

DOL-DETFPi Electrolyte Precursor Solution

3.5 g of DOL, 5.9 g of EC/DMC, 0.5 g of TTE, and 0.1 g of DETFPi were mixed thoroughly in a 20 mL sample bottle. Subsequently, 0.94 g of $LiBF_4$ was dissolved in 10 mL of DOL/EC/DMC/TTE/DETFPi solution with stirring until complete dissolution to obtain the precursor solution.

Electrode Preparation

NCM811 Cathode

$LiNi_{0.8}Co_{0.1}Mn_{0.1}O_2$, Super-P, and PVDF were dispersed in NMP at a mass ratio of 84:10:6 to achieve a mixture with a solid content of 20%. The mixture was blade-coated evenly onto an aluminum foil (16 μm), then dried in a convection oven at 60 °C for 7 hours, Afterwards, it was subjected to hot pressing at 80 °C, followed by drying in a vacuum oven at 120 °C for 12 hours to obtain NCM811 cathode sheets with a thickness of approximately 80 μm (active material loading of 7.2 mg cm^{-2}). The sheets were cut into circular pieces with a diameter of 13 mm and transferred to a glove box for further use.

Graphite Anode

Graphite anodes were purchased from Shenzhen Kejing Zhida Technology Co., Ltd. They were cut into circular pieces with a diameter of 15 mm, and vacuum-dried at 100 °C for 6 hours before being transferred to a glove box for use.

Battery Assembly

NCM811||Li Battery

All button batteries were assembled in an argon-filled glove box. NCM811, LATP/PE/LATP and lithium metal were used as the cathode, separator and anode, respectively. To start with 100 μL of the in-situ polymerization precursor solution was added to each button battery. The batteries were sealed and left at room temperature for 24 hours for polymerization to obtain the in-situ solidified NCM811||Li battery. The reference batteries were assembled similarly but with PE separators.

NCM811||C Battery

NCM811, LATP/PE/LATP, and graphite were used as the cathode, separator and anode, respectively. Similar to the NCM811||Li battery, 100 μL of the in-situ polymerization precursor solution was added to each button battery. The batteries were sealed and left at room temperature for 24 hours for polymerization to obtain the in-situ solidified NCM811||C battery. The reference batteries used PE separators in contrast.

The electrolyte obtained after in-situ polymerization of the precursor solution supported by the LATP/PE/LATP composite separator was labeled as PDOL@LATP electrolyte, while the reference electrolytes were labeled as PDOL@PE.

Characterization and Measurement

The morphology of electrodes and electrolytes was characterized using scanning electron microscopy (SEM, Hitachi S4800). The particle size distribution of LATP particles was determined using a nanoparticle size analyzer. Contact angles were measured using a German Dataphysics OCA20 video optical contact angle measurement system.

The various properties of the electrolyte were measured using a Germany Zennium 6 electrochemical workstation. Ion conductivity was determined using electrochemical impedance spectroscopy (EIS) and calculated accordingly. The electrochemical stability window was measured by linear sweep voltammetry (LSV).[28] The lithium ion transference number was measured using the Bruce Evans Vincent method: a DC polarization voltage ($\Delta V = 10$ mV) was applied to the battery, and initial and steady-state currents were recorded. AC impedance spectroscopy before and after polarization was measured using an electrochemical workstation, and the lithium ion transference number was calculated using the BEV equation.[28]

Battery performance was tested at room temperature using a Land 2001 A battery testing system. For NCM811||Li and NCM811||C (1 C = 200 mA g^{-1}) batteries, the voltage range tested was 3.0–4.35 V.

Results and Discussion

LATP Particle Size and Composite Film Structure Characteristics

The particle size of LATP not only directly affects the diffusion rate of ions within the separator, which is crucial for the interface properties between the separator and electrodes. Smaller particle sizes typically suggest higher surface area and shorter diffusion paths, potentially enhances ion transport rates. Appropriate particle sizes can promote better ion exchange, improving the electrochemical and charge-discharge performance of batteries. The particle size and distribution of LATP particles in the slurry system were measured using a nanoparticle size analyzer (Figure S1). The sizes of smaller particles ranged from 120–500 nm, while larger particles ranged from 500–1100 nm.

LATP/PE/LATP composite separator was fabricated by symmetrically coating LATP slurry on both sides of a PE separator. The surface and cross-sectional SEM images of the composite separator are shown in Figure 1a and b. It can be observed that the surface of the LATP/PE/LATP composite separator is fully covered with LATP particles, and there are numerous micropores between particles, facilitating the infiltration of DOL and enhancing the subsequent in-situ solidification effects. The composite separator exhibits a sandwich-like structure, with a PE separator thickness of 9 μm and a total thickness of 15 μm after applying a 3 μm layer of LATP on each side.

During the in-situ polymerization process, the wettability between the precursor solution and the substrate during the in-

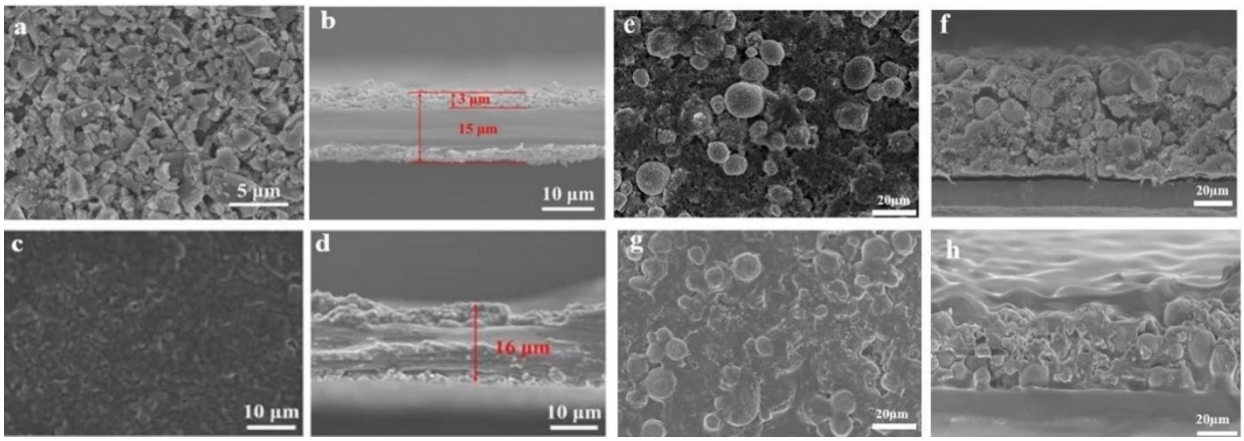

Figure 1. SEM images of the surface and cross section of the LATP/PE/LATP separator (a, b) before and (c, d) after in situ polymerization. SEM images of the surface and cross section of the cathode (e, f) before and (g, h) after in situ polymerization, respectively.

situ polymerization process affects the interfacial properties between the electrolyte and the substrate. The wetting behaviors of LATP coatings on PE separator and LATP/PE/LATP composite separator with DOL precursor solution were tested, as shown in Figure S2. The contact angle between the PE separator and DOL precursor solution was measured at 29.5°, while that of the LATP/PE/LATP composite separator with the DOL precursor solution was 7.2°. This indicates that the LATP coating enhances the wettability between the separator and the precursor solution, facilitating the infiltration of the precursor solution into LATP particles and the composite separator for the polymerization.

Characteristics of PDOL-LATP Electrolyte

The LATP/PE/LATP composite separator was assembled into a battery, and after injecting the DOL precursor solution to initiate its in-situ polymerization, the PDOL@LATP composite electrolyte was obtained. After in-situ polymerization, LATP particles on the surface of the composite separator were completely covered by the in-situ polymerized DOL (Figure 1c). The cross-section SEM images of composite electrolyte (Figure 1d) demonstrate that PDOL has penetrated deeply into the internal voids of the LATP layer. The fixed LATP coating effectively avoids the uneven distribution of inorganic particles which is typically found in conventional composite electrolytes. SEM images of the NCM811 cathode before and after in-situ polymerization (Figure 1e–f) show that DOL has infiltrated into the interior of cathode particles and polymerized in situ, covering both the surface and interior of the cathode with the in-situ polymerized DOL electrolyte, thereby ensuring good interface contact.

Ionic conductivity reflects the ion conduction ability of solid electrolytes. The ionic conductivities of PDOL@PE and PDOL@LATP electrolytes were tested using symmetrical cells with stainless steel blocking electrodes. The AC impedance spectra of PDOL@PE and PDOL@LATP electrolytes at room temperature are shown in Figure 2a. The calculated ionic conductivities of PDOL@PE and PDOL@LATP electrolytes are 1.29×10^{-4} S cm^{-1} and 1.59×10^{-4} S cm^{-1}, respectively. As can be seen, the introduction of LATP particles enhances the lithium ion conductivity of the PDOL electrolyte.

The temperature dependence of the ionic conductivity of in-situ polymerized composite electrolytes was tested in the range of 30–80 °C, as shown in Figure 2b. The ionic conductivity of the electrolyte increases with the increase of temperature. The activation energy (E_a) calculated for PDOL@PE electrolyte is 13.36 kJ mol^{-1}, while that for PDOL@LATP electrolyte is 12.22 kJ mol^{-1}, indicating there was less hindrance to ion movement in the composite electrolyte. The migration of lithium ions in PDOL involves is achieved through the movement of polymer chain segments after the coordination of lithium ions and oxygen atoms in PDOL. Generally, there are three migration pathways for lithium ions in organic/inorganic composite electrolytes: migration along polymer chains, migration through inorganic electrolytes, and migration at organic/inorganic interfaces. Lithium ion conductivity of PDOL@LATP electrolyte is higher than that of PDOL@PE electrolyte, while the activation energy for lithium ion migration is lower than

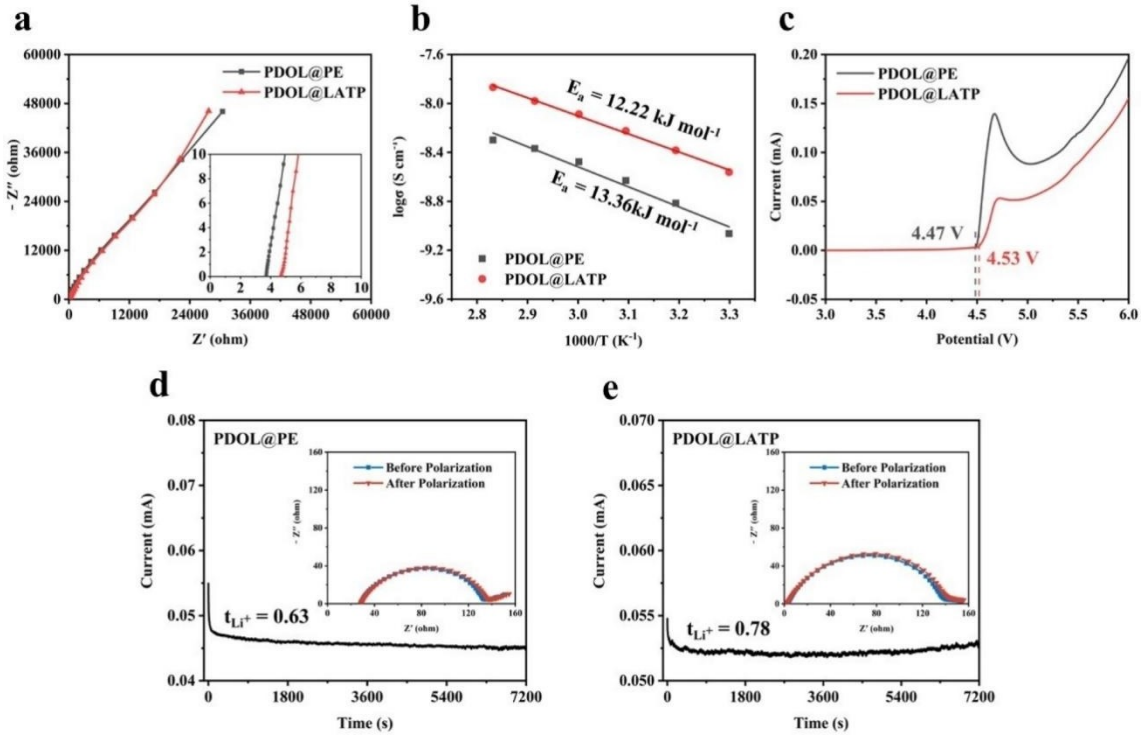

Figure 2. Electrochemical characteristics of the two electrolytes: (a) Nyquist plot, (b) Arrhenius plot of ion conductivity and temperature, and (c) Linear sweep voltammetry curves; Chrono current curves of (d) PDOL@PE and (e) PDOL@LATP. (with inset of EIS spectra before and after polarization).

Research Article
doi.org/10.1002/batt.202400463
Chemistry Europe
European Chemical Societies Publishing

that of PDOL@PE electrolyte. Therefore, it can be concluded that the synergistic effect of PDOL and LATP electrolyte promotes the effective transfer of lithium ions in PDOL@LATP electrolyte.

The solid-state electrolyte electrochemical window is crucial for the long-term operation of high voltage or high energy density battery systems. Two types of electrolyte membranes were tested using linear sweep voltammetry (LSV), and the results are shown in Figure 2c. The oxidation voltage of PDOL@PE and PDOL@LATP are 4.47 V and 4.53 V, respectively. The enhanced oxidation stability enables PDOL@PE and PDOL@LATP to work under high voltage battery systems.

The time-current curve and EIS spectra before and after polarization were obtained by testing the lithium symmetric battery using steady-state polarization method (Figure 2d and 2e), and the lithium ion migration numbers of the two electrolytes were calculated thereby. The lithium ion migration number of PDOL@LATP is 0.78, which is higher than that of PDOL@PE (0.60). High lithium ion migration number is beneficial for improvingthe rate performance of batteries by reducing concentration polarization near the anodes to avoid the generation of lithium dendrites.

Battery Application Evaluation

NCM811||Li Battery System

NCM811||Li batteries were assembled using PE separator and LATP/PE/LATP composite separator, followed by in-situ curing and testing. The cycling performance in the voltage range of 3.0–4.35 V at 1 C is shown in Figure 3a, with the corresponding charge-discharge curves in Figures 3b and 3c. The initial discharge capacity of NCM811||PDOL@PE||Li battery was 186.9 mAh g^{-1}, with rapid capacity decay after 200 cycles, and retaining 95.0 mAh g^{-1} retaining after 500 cycles (capacity retention of 50.9%). In contrast, NCM811||PDOL@LATP||Li battery exhibited superior cycling performance with an initial capacity of 187.6 mAh g^{-1}. After 500 cycles, it still retained 153.9 mAh g^{-1} (82.1% capacity retention), with a coulombic efficiency of up to 99.7%. Furthermore, NCM811||PDOL@PE||Li battery showed faster voltage polarization with increasing cycle numbers (Figure 3b), while NCM811||PDOL@LATP||Li battery exhibited lower voltage polarization (Figure 3c). Clearly, PDOL@PE electrolyte showed poorer stability of lithium under higher current density, which not only led to lithium dendrite formation and dead lithium, but also increased interface resistance and caused higher polarization as well, thus resulting in faster capacity decay. Comparatively, batteries with LATP-coated PE separator and in-situ solidified DOL demonstrated stable cycling at 1 C rate. It proves that LATP coating facilitates lithium ion migration, thereby enhancing the lithium ion conductivity of the solid electrolyte.

Rate performance test results (Figure 3d) indicated that NCM811||PDOL@LATP||Li battery achieved discharge capacities of 209.7, 204.5, 195.8, 186.5, and 174.9 mAh g^{-1} at 0.1, 0.2, 0.5, 1.0, and 2.0 C rates, respectively, higher than those of NCM811||PDOL@PE||Li battery. The capacity difference between the two batteries widened notably, especially at 1 C and 2 C rates. When it returned to to 0.1 C rate, the discharge capacity restored to its initial level. These results demonstrate that NCM811||PDOL@LATP||Li battery exhibits superior rate capability and long-term cycling stability.

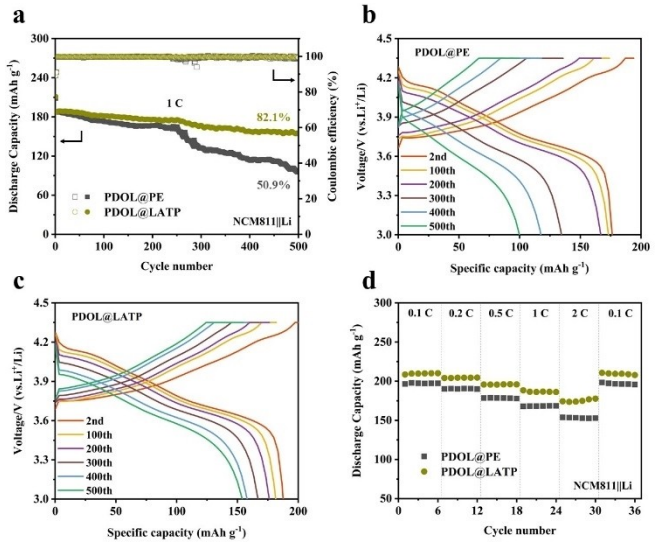

Figure 3. (a) Cycling performances and Coulombic efficiencies of NCM811||PDOL@PE||Li and NCM811||PDOL@LATP||Li batteries; (b, c) Charge and discharge profiles of NCM811||PDOL@PE||Li and NCM811||PDOL@LATP||Li batteries at different cycles; (d) Rate performance of NCM811||PDOL@PE||Li and NCM811||PDOL@LATP||Li batteries.

NCM811||C System

To evaluate the practicality of the composite electrolyte in full cells, we assembled NCM811||C batteries and tested them after in-situ curing, with an N/P ratio of 1.12. The cycling performance at 0.5 C rate in the voltage range of 3.0–4.35 V is shown in Figure 4a. The initial discharge capacity of NCM811||PDOL@PE||C battery was 166.8 mAh g^{-1}, with 130.4 mAh g^{-1} remaining after 200 cycles (capacity retention of 78.2%). In comparison, NCM811||PDOL@LATP||C battery exhibited an initial discharge capacity of 174.1 mAh g^{-1}, with 138.3 mAh g^{-1} remaining after 200 cycles (capacity retention of 79.4%).

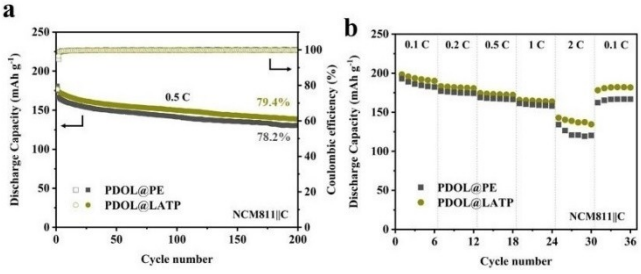

Figure 4. (a) Cycling performances (b) rate performances of NCM811||PDOL@PE||C and NCM811||PDOL@LATP||C batteries.

Research Article
doi.org/10.1002/batt.202400463
Chemistry Europe
European Chemical Societies Publishing

Rate performance of solid-state batteries is depicted in Figure 4b. NCM811||PDOL@LATP||C battery achieved discharge capacities of 193.6, 181.9, 172.8, 164.9, and 138.9 mAh g^{-1} at 0.1, 0.2, 0.5, 1.0, and 2.0 C rates, respectively, all higher than those of NCM811||PDOL@PE||C battery. Particularly at 2 C rate, NCM811||PDOL@LATP||C battery demonstrated a more significant capacity advantage. When it returned to 0.1 C, the discharge capacity recovered close to the initial level.

Our previous study[32] concluded that during battery cycling, DETFPi in the electrolyte preferentially oxidizes on the cathode surface, forming a thin and uniform CEI layer that suppresses the decomposition of PDOL and other components, thereby enhancing the cycling performance of battery. Simultaneously, it reduces interfacial impedance, thereby improving rate capability. We explored further in this work, and developed a dual electrolyte system combining organic (PDOL) and inorganic (LATP ion conductor) components by firstly coating LATP ion conductor on PE separators and then in-situ polymerizing with DOL. In the dual electrolyte system, lithium ion transports across the polymer electrolyte, LATP ion conductor, and their interface within this system. It enhances lithium ion conductivity and migration number, facilitates rapid lithium ion transport and reduces resistance, thereby improving both the cycling and rate performance of the battery.

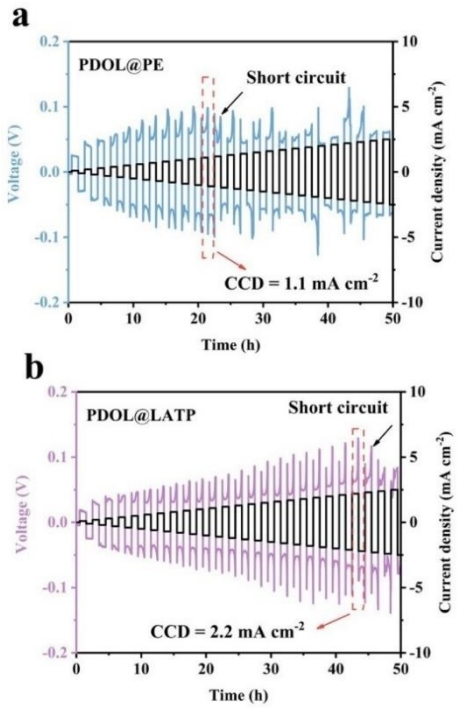

Figure 5. Critical current density of (a) PDOL@PE and (b) PDOL@LATP.

Electrolyte/Lithium Metal Interface Characteristics

The interface stability and dendrite suppression capability of PDOL@PE and PDOL@LATP electrolytes were evaluated using lithium symmetric cells. Critical current density (CCD) is a method for evaluating the maximum current density that lithium batteries can withstand. Lithium||PDOL@PE||Li and Lithium||PDOL@LATP||Li symmetric batteries were assembled and tested for critical current density. The results show that both PDOL@PE (Figure 5a) and PDOL@LATP (Figure 5b) exhibited stable polarization voltage platforms, which reached up to 0.5 mA cm^{-2}, hence indicating the good lithium plating/stripping performance. However, as the current density increased gradually, PDOL@PE showed sharp peaks in polarization voltage platform, due to the formation of dead lithium and dendrites. PDOL@PE exhibited unstable polarization voltage platform at 1.1 mA cm^{-2}. Failing to meet the conditions for normal operation at this current density, it reached its CCD. In contrast, PDOL@LATP maintained a relatively stable polarization voltage, reaching up to 2.2 mA cm^{-2}, with its CCD not less than 2.2 mA cm^{-2}. The CCD of PDOL@LATP was twice that of PDOL@PE,indicating significantly improved stability. This suggests that batteries using PDOL@LATP electrolyte can operate at higher current densities, which means, it exhibits significantly improved rate capability.

In long-term constant current cycling of Li||Li symmetric cells, the interface stability between the electrolyte and lithium metal was evaluated. As shown in Figures 6a and 6b, at a current density of 0.5 mA cm^{-2}, the overpotential of the Li||PDOL@PE||Li battery gradually stabilized from an initial

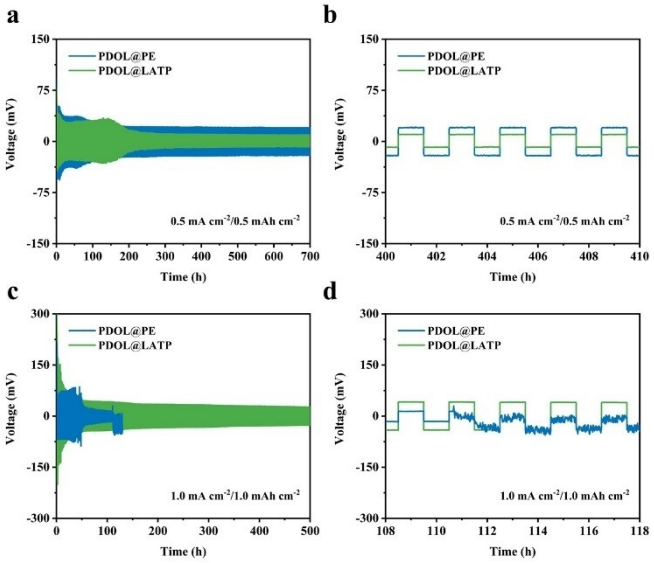

Figure 6. Li||Li batteries assembled with two electrolyte : (a) Galvanostatic cycling curves at 0.5 mA cm−2/0.5 mAh cm−2 and (b) magnified voltage profile from 300–310 h; (c) Galvanostatic cycling curves at 1.0 mA cm−2/1.0 mAh cm−2 and (b) magnified voltage profile from 108–118 h.

51.2 mV–20 mV after 200 h, and it maintained stable cycling for over 500 h. In comparison, Li||PDOL@LATP||Li battery exhibited a similar trend but with a lower overpotential of 10 mV. Furthermore, when the test current density was increased to 1.0 mA cm^{-2}, Li||PDOL@PE||Li battery showed micro-short circuits after 50 h and failed after 110 h. In contrast, Li||PDOL@LATP||Li battery maintained stable cycling with an overpotential of 35 mV for over 500 h, as depicted in Figures 6c

and 6d. These results demonstrate that the Li symmetric battery based on PDOL@LATP has better dendrite suppression capability and stability during long-term cycling with lithium metal.

To investigate the effects of the electrolytes on the morphology of lithium deposition, Li||Li symmetric batteries were disassembled after 50 cycles at 1.0 mA cm^{-2}/1.0 mAh cm^{-2}, and the surface morphology of the lithium anode was observed using SEM. As illustrated in Figures 7a and 7b, the surface of lithium anode in Li||PDOL@PE||Li battery exhibited a black, uneven surface layer, whereas in Li||PDOL@LATP||Li battery, the lithium anode took on silver-gray and smooth surface. SEM images revealed that the lithium surface in Li||PDOL@PE||Li battery was uneven with numerous pores, and dendrites were observed in high-magnification SEM images (Figure 7c). On the contrary, no dendrites were observed on the lithium surface of Li||PDOL@LATP||Li battery (Figure 7d).

Synergy of PDOL and LATP in Improving the Battery Performance

Comparing the results of this study with the previously reported data, we found that the performance of PDOL batteries is significantly improved compared with batteries using liquid electrolytes; The performance of PDOL-LATP batteries is even much better than that of PDOL batteries. This indicates that PDOL and LATP have exerted a synergistic effect on improving battery performance. The comparative data is presented in Table 1.

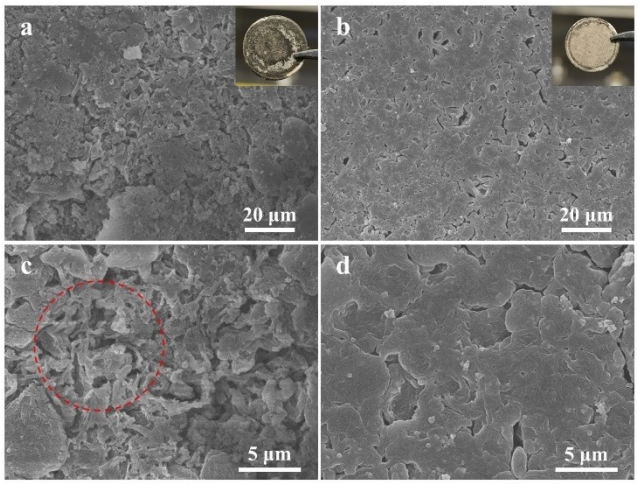

Figure 7. (a) SEM images of the lithium anode surface of Li||PDOL@PE||Li cell and (b) Li||PDOL@LATP||Li cell after 50 cycles of galvanostatic cycling at 1.0 mA cm−2/1.0 mAh cm−2 (inset is a digital photograph of the post-cycling lithium anode); (c) and (d) are the corresponding magnified SEM images.

Conclusions

DOL-DETFPi is an effective in-situ solid-state electrolyte that can improve the electrochemical performance, cycling stability, and inhibit the formation of lithium dendrites in NCM811 batteries. DOL-DETFPi infiltrates into the gaps between LATP particles in the separator coating, and after in-situ polymerization, forms a composite solid electrolyte layer with LATP. This composite electrolyte exhibits significantly better ion conductivity and more lithium ion migration number than that of PDOL@PE electrolyte.

Moreover, PDOL@LATP composite electrolyte exhibits higher discharge capacity and stability at high rates, significantly improving the performance of PDOL @ PE batteries. Lastly, in lithium symmetric batteries, PDOL@LATP composite electrolyte shows lower overpotential and stable dendrite suppression ability in lithium symmetric batteries, which greatly improves the safety and cycle life of the battery.

Supporting Information Summary

Particle size distribution of LATP particles; Contact angles of precursor solutions on different separator: (a) LATP/PE/LATP composite separator and (b) PE separator.

Acknowledgements

This work was financially supported by the National Key R&D Pilot Project "Research and development of high temperature resistant, long life and high safety lithium batteries" (2022YFE0207300). We thank Ms. Wang for translating this article.

Conflict of Interests

The authors declare no conflict of interest.

Table 1. Cycling performance of NCM811||Li with different electrolytes.

Electrolyte	conductivity/×10^{-4} S/cm	t_{Li+}	CCD/mA·cm^{-2}	Number of cycles	Capacity retention	Ref.
LE [a]	2.36	0.48	–	300@0.5 C	63%	[32]
PDOL	1.27	0.53	–	300@0.5 C	66%	[32]
PDOL@PE	1.29	0.60	1.1	500@1 C	50.9%	This work
PDOL@LATP	1.59	0.78	2.2	500@1 C	82.1%	This work

[a] 1 mol/L $LiBF_4$-DMC-EC (DMC/EC = 7/3, w/w)

Data Availability Statement

The data that support the findings of this study are available from the corresponding author upon reasonable request.

Keywords: In-situ polymerization · Polydioxolane · Sacrificial additives · LATP/PE/LATP separator · High-voltage lithium battery

[1] Z. Zhang, W. Q. Han, *Nano-Micro Lett.* **2024**, *16*, 24.
[2] Z. Wang, J. Liu, M. Wang, X. Shen, T. Qian, C. Yan, *Nanoscale Adv.* **2020**, *2*, 1828–1836.
[3] C. Li, Z. Wang, Z. He, Y. Li, J. Mao, K. Dai, C. Yan, J. Zheng, *Sustain. Mater. Techno.* **2021**, *29*, e00297.
[4] C. Yang, K. Fu, Y. Zhang, E. Hitz, L. Hu, *Adv. Mater.* **2017**, *29*, 1701169.
[5] J. Hu, Y. C. Gao, S. J. Yang, X. L. Wang, X. Chen, Y. L. Liao, S. Li, J. Liu, H. Yuan, J. Q. Huang, *Adv. Funct. Mater.* **2024**, *34*, 2311633.
[6] J. F. Wu, R. Zhang, Q. F. Fu, J. S. Zhang, X. Y. Zhou, P. Gao, C. H. Xu, J. Liu, X. Guo, *Adv. Funct. Mater.* **2021**, *31*, 2008165.
[7] Y. Hu, X. Xie, W. Li, Q. Huang, H. Huang, S. M. Hao, L. Z. Fan, W. Zhou, *ACS Sustainable Chem. Eng.* **2023**, *11*, 1253–1277.
[8] H. Liang, L. Wang, A. Wang, Y. Song, Y. Wu, Y. Yang, X. He, *Nano-Micro Lett.* **2023**, *15*, 42.
[9] Y. Zheng, Y. Yao, J. Ou, M. Li, D. Luo, H. Dou, Z. Li, K. Amine, A. Yu, Z. Chen, *Chem. Soc. Rev.* **2020**, *49*, 8790–8839.
[10] S. Luo, X. Liu, L. Gao, N. Deng, X. Sun, Y. Li, Q. Zeng, H. Wang, B. Cheng, W. Kang, *Sustain. Energy Fuels* **2022**, *6*, 5019–5044.
[11] H. Wang, S. Duan, Y. Zheng, L. Qian, C. Liao, L. Dong, H. Guo, C. Ma, W. Yan, J. Zhang, *eTransportation* **2024**, *20*, 100311.
[12] L. He, J. H. Cao, Y. K. Wang, D. Y. Wu, *Energy Adv.* **2022**, *1*, 1028.
[13] L. He, W. H. Liang, J. H. Cao, D. Y. Wu, *ACS Appl. Energ. Mater.* **2022**, *5*, 5277–5286.
[14] S. Zhang, B. Xie, X. Zhuang, S. Wang, L. Qiao, S. Dong, J. Ma, Q. Zhou, H. Zhang, J. Zhang, J. Ju, G. Xu, Z. Cui, G. Cui, *Adv. Funct. Mater.* **2024**, *34*, 2314063.
[15] H. Peng, T. Long, J. Peng, H. Chen, L. Ji, H. Sun, L. Huang, S. G. Sun, *Adv. Energy Mater.* **2024**, *14*, 2400428.
[16] G. Xiao, H. Xu, C. Bai, M. Liu, Y. B. He, *Interdiscip. Mater.* **2023**, *2*, 609–634.
[17] Q. Liu, L. Wang, X. He, *Adv. Energy Mater.* **2023**, *13*, 2300798.
[18] V. Vijayakumar, B. Anothumakkool, S. Kurungot, M. Winter, J. R. Nair, *Energy Environ. Sci.* **2021**, *14*, 2708–2788.
[19] H. Yang, M. Jing, L. Wang, H. Xu, X. Yan, X. He, *Nano-Micro Lett.* **2024**, *16*, 217.
[20] B. H. Zhang, W. X. Wen, H. Y. Wang, Y. L. Hou, J. Z. Chen, D. L. Zhao, *Chem. Eng. J.* **2023**, *472*, 144990.
[21] T. Yang, W. Zhang, Y. Liu, J. Zheng, Y. Xia, X. Tao, Y. Wang, X. Xia, H. Huang, Y. Gan, X. He, J. Zhang, *Small* **2023**, *19*, 2303210.
[22] J. Ma, Y. Wu, H. Jiang, X. Yao, F. Zhang, X. Hou, X. Feng, H. Xiang, *Energy Environ. Mater.* **2022**, *6*, e12370.
[23] Z. Wang, Y. Wang, L. Shen, Z. Jin, H. M. Law, A. Wang, W. Wang, F. Ciucci, *Energy Environ. Sci.* **2023**, *16*, 4084–4092.
[24] Y. Bai, W. Ma, W. Dong, Y. Wu, X. Wang, F. Huang, *ACS Appl. Mater. Interfaces* **2023**, *15*, 26834–26842.
[25] Q. Hao, Y. Gao, F. Chen, X. Chen, Y. Qi, N. Li, *Chem. Eng. J.* **2024**, *481*, 148666.
[26] A. Hu, Z. Liao, J. Huang, Y. Zhang, Q. Yang, Z. Zhang, L. Yang, S. Hirano, *Chem. Eng. J.* **2022**, *448*, 137661.
[27] S. Qin, Y. Yu, J. Zhang, Y. Ren, C. Sun, S. Zhang, L. Zhang, W. Hu, H. Yang, D. Yang, *Adv. Energy Mater.* **2023**, *13*, 2301470.
[28] L. Y. Yang, J. H. Cao, W. H. Liang, Y. K. Wang, D. Y. Wu, *ACS Appl. Mater. Interfaces* **2022**, *14* (11), 13722–13732.
[29] T. Liang, J. H. Cao, W. H. Liang, Q. Li, L. He, D. Y. Wu, *RSC Adv.* **2019**, *9*, 41151–41160.
[30] J. Liu, J. Cao, W. Liang, L. Yang, D. Wu, *ACS Appl. Polym. Mater.* **2022**, *4*(5), 4003–4012.
[31] M. Sun, Z. Zeng, W. Zhong, Z. Han, L. Peng, S. Cheng, J. Xie, *Batteries & Supercaps* **2022**, *5* (12), e202200338.
[32] P. Zhang, J. H. Cao, W. H. Liang, Y. Li, Y. K. Wang, D. Y. Wu, *ACS Appl. Energ. Mater.* **2024**, *7*, 4088–4100.
[33] J. Zhang, Y. Su, Y. Qiu, X. Zhang, F. Xu, H. Wang, *ACS Appl. Mater. Interfaces* **2024**, *16* (23), 30128–30136.
[34] L. Pan, S. Feng, H. Sun, X. X. Liu, P. Yuan, M. Cao, M. Gao, Y. Wang, Z. Sun, *Small* **2024**, *20*, 2400272.
[35] H. Zhang, J. Gou, K. Cui, X. Zhang, Y. Yao, S. Wang, H. Wang, *Nano-Micro Lett.* **2024**, *16*, 181.
[36] S. Li, J. Lu, Z. Geng, Y. Chen, X. Yu, M. He, H. Li, *ACS Appl. Mater. Interfaces* **2022**, *14*, 1195–1202.
[37] B. Cao, Y. Huang, W. Cao, K. Zhou, Z. Geng, H. Li, *ACS Appl. Energ. Mater.* **2023**, *6*, 8626–8633.

Manuscript received: July 6, 2024
Revised manuscript received: August 7, 2024
Version of record online: October 15, 2024